THE JOURNAL OF PHYSICAL CHEMISTRY B

Article

Cite This: J. Phys. Chem. B 2017, 121, 10118-10124

pubs.acs.org/JPCB

Persistent Self-Association of Solute Molecules in Solution

Weiwei Tang,[†] Huaping Mo,[§] Mingtao Zhang,[‡] Sean Parkin,[∥] Junbo Gong,*[,†] Jingkang Wang,[†] and Tonglei Li*[,‡]

[†]School of Chemical Engineering and Technology, State Key Laboratory of Chemical Engineering, The Co-Innovation Center of Chemistry and Chemical Engineering of Tianjin, Tianjin University, Tianjin 300072, People's Republic of China

[‡]Department of Industrial and Physical Pharmacy, College of Pharmacy, Purdue University, West Lafayette, Indiana 47907, United States

[§]Department of Medicinal Chemistry and Molecular Pharmacology, College of Pharmacy, Purdue University, West Lafayette, Indiana 47907, United States

[∥]X-ray Facility, Department of Chemistry, University of Kentucky, Lexington, Kentucky 40506, United States

Supporting Information

ABSTRACT: The structural evolvement of a solute determines the crystallization outcome. The self-association mechanism leading to nucleation, however, remains poorly understood. Our current study explored the solution chemistry of a model compound, tolfenamic acid (TFA), in three different solvents mainly by solution NMR. It was found that hydrogen-bonded pairs of solute−solute or solute−solvent stack with each through forming a much weaker $\pi-\pi$ interaction as the concentration increases. Depending on the solvent, configurations of the solution species may be retained in the resultant crystal structure or undergo rearrangement. Yet, the $\pi-\pi$ stacking is always retained in the crystal regardless of the solvent used for the crystallization. The finding suggests that nucleation not only involves the primary intermolecular interaction (hydrogen bonding) but also engages the secondary forces in the self-assembly process.

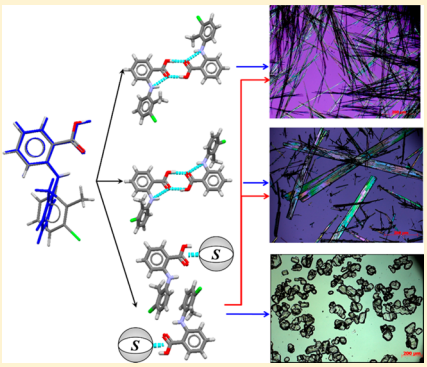

INTRODUCTION

Crystallization from solution plays a fundamental role in various natural and industrial processes.[1,2] Its mechanism at the molecular level remains to be explored. Experimental observation of structure resemblance between solution chemistry and final crystal structure has shed light on possible molecular events involved during nucleation.[3−9] In our earlier studies of TFA, we concluded that solute molecules self-associate in ethanol by bifurcated hydrogen bonds between their carboxyl groups and believed that the hydrogen-bonded dimers in solution form basic nucleation units carried into the crystal forms. This conclusion was recently challenged and the link between solution chemistry and crystallization outcome questioned.[10] Herein, we conducted detailed studies of self-assembly of TFA in three distinct solvents: ethanol, dimethylformamide (DMF), and toluene. We envisaged that the difference in solvent−solute and solute−solute interactions among three solvents could further clarify the role of intermolecular interactions in crystal formation.

TFA (Figure 1) is a nonsteroidal anti-inflammatory drug (NSAID) and displays conformational polymorphism including five structurally solved polymorphs.[11,12] Forms I and II are the most encountered, whereas forms III, IV, and V were only obtained with polymers used as heteronuclei.[12] The conformations of polymorphs I and II differ mainly in the torsion angle τ (Figure 1), which is ±74.9° in form I and ±142.6° in II.

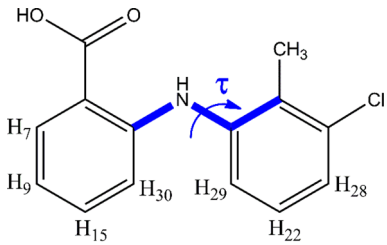

Figure 1. Molecular structure of TFA along with the ^{1}H NMR proton labeling scheme. The major torsion angle, τ, is also marked.

These are referred to as "twisted-like" (TL) and "planar-like" (PL), respectively. The same intermolecular hydrogen bonding ($R_2^2(8)$) between neighboring carboxyl groups is present in both polymorphs (Figure 2a). The hydrogen-bonding motif is complemented in the crystal by $\pi\cdots\pi$ face-to-face and $-CH\cdots\pi$ face-to-edge interactions.

EXPERIMENTAL AND COMPUTATIONAL SECTIONS

Materials. Tolfenamic acid (>97% purity) was purchased from TCI America (Portland, OR). *N*,*N*-Dimethylformamide

Received: August 4, 2017
Revised: October 2, 2017
Published: October 10, 2017

DOI: 10.1021/acs.jpcb.7b07763
J. Phys. Chem. B 2017, 121, 10118−10124

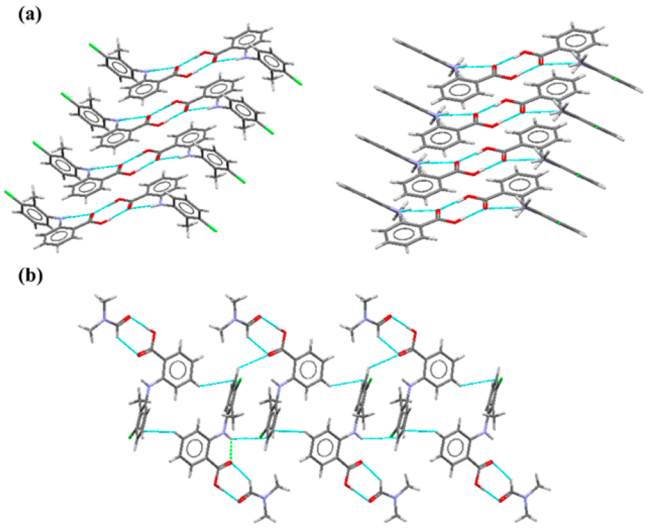

Figure 2. Crystal structures of forms I (a, left) and II (a, right) and DMF solvate (b).

(DMF; ≥99.8% purity) was purchased from Avantor Performance Materials Inc. (Center Valley, PA) and Fisher Scientific (Fair Lawn, NJ), toluene (≥99.5% purity) from Fisher Scientific (Fair Lawn, NJ), and ethanol (≥99.9% purity) from Decon Laboratories, Inc. (King of Prussia, PA). DMF-d_7 (99.5% D), toluene-d_8 (99.5% D), and ethanol-d_6 (99% D, anhydrous) were purchased from Cambridge Isotope Laboratories, Inc. (Andover, MA), and tetramethylsilane (TMS, NMR grade) was from Acros Organics (Fair Lawn, NJ).

Crystal Structure Determination. The structure of single crystals of TFA DMF solvate was determined by single-crystal X-ray diffraction. Crystals were grown by slow evaporation of DMF solutions (8.20 mg of TFA/1 mL DMF) at 295 K over several days. Data collection was conducted at 90 K on a Nonius kappa CCD diffractometer (Mo Kα, λ = 0.71073 Å). Powder X-ray diffraction (PXRD) measurements were carried out on a Rigaku X-ray diffractometer (Cu Kα, λ = 1.5406 Å) from 5.0° to 40.0° at a scan rate of 8°/min.

FTIR Spectroscopy. FTIR spectra were recorded on a Cary 600 Series FTIR spectrometer (Agilent Technologies Inc.) in conjunction with Agilent Resolutions Pro v5.2 software, equipped with PIKE MIRacle ATR ZnSe and Multi Reflection HATR accessories for handling solid and solution samples, respectively. For each sample, 32 scans were collected over a spectral region from 800 to 1800 cm^{-1} at a resolution of 2 cm^{-1} and from 740 to 790 cm^{-1} with 0.5 cm^{-1} resolution.

NMR Spectroscopy. ^{1}H NMR and two-dimensional (2D) NMR spectra were acquired either on an 800 MHz Bruker Avance-III spectrometer or on a 500 MHz Bruker Avance spectrometer at 298 K. Data were processed and analyzed using TOPSPIN software. NMR samples were prepared by diluting a known concentration of TFA solutions in DMF-d_7, ethanol-d_6, and toluene-d_8, respectively. ^{1}H NMR spectra were acquired with scan numbers varying from 32 to 256. Chemical shifts were referenced to tetramethylsilane (TMS), at 0.00 ppm. Proton chemical shifts in ethanol-d_6 were measured three times.

Heteronuclear Multiple Bond Correlation (HMBC) Spectroscopy. 2D HMBC spectra were acquired at a range of concentrations of TFA in DMF-d_7, ethanol-d_6, and toluene-d_8, respectively, to determine carboxyl ^{13}C chemical shifts. The spectral width for ^{1}H channel (F2 dimension) is 11 ppm and for ^{13}C (F1) varies from 5 to 1 ppm, centered at 170.5 ppm. Depending upon the measured concentration, acquisition times were 0.12 s (^{1}H) and 0.13−0.16 s (^{13}C), and the number of scans ranged from 2 to 128. ^{1}H and ^{13}C chemical shifts were both referenced to TMS. A typical measurement of C═O ^{13}C shift in HMBC spectrum is shown in Figure S3. The concentrations of TFA in three solvents were verified and redetermined by the peak integration of proton H_{30} relative to that of the initially prepared sample.

Nuclear Overhauser Effect Spectroscopy (NOESY). 2D NOESY experiments were carried out for TFA solutions in DMF-d_7, ethanol-d_6, and toluene-d_8 at 298 K. 2D NOE spectra were acquired with a standard pulse over a sweep width of 16 ppm in DMF-d_7, and 11 ppm in ethanol-d_6 and toluene-d_8 for both F1 and F2 dimensions. The number of F1 increment was 256 or 128, each with 4096 data points in the F2 dimension. Nuclear Overhauser effect (NOE) mixing time was optimized as 0.8 s by measuring NOE buildups,[13] and a relaxation delay of 9 s was applied. Numbers of scans and dummy scans were both set to 16. Cross-peak volumes were measured with TOPSPIN software (version 2.1), and a square region enclosing each pertinent cross-peak was chosen, and the peak volume was read. Spectral noise (i.e., the error in peak volume determination) was estimated by integrating similar adjacent areas that contain no signal and subtracting from the cross- and diagonal-peak volumes. Diagonal peak volumes were divided by their values at the lowest concentrations of TFA to obtain the scaling factor, which was used for normalizing cross-peak volumes to correct for concentration effects.[14] Finally, cross-peak volumes were divided by a reference cross-peak volume to account for changes in molecular conformation and/or self-association. 2D NOESY at each concentration was measured at least twice in toluene-d_8 and DMF-d_7, and at least once in ethanol-d_6.

Energy Calculation. Density functional theory (DFT) calculations were performed using the Gaussian 09 package.[15] The geometries of TFA monomer, TFA−solvent complex (solvated monomer), dimer, and solvated dimer models were retrieved from crystal structures of TFA polymorphs I and II and DMF solvate and further optimized at the B97D/6-31+G(d,p) theory using SMD implicit solvation model.[16] The binding energy accounts for both conformation change and intermolecular interaction upon formation of a TFA-solvent complex or TFA-TFA dimer

$$\Delta E_{\text{bind}} = E_{\text{A-B}} - E_{\text{A}} - E_{\text{B}} \quad (1)$$

where $E_{\text{A-B}}$ is the total energy of a TFA-solvent complex or TFA−TFA dimer, E_{A} is the energy of the optimized TFA molecule with planar-like (PL) conformation, and E_{B} is the energy of the optimized solvent molecule or TFA molecule. A further single-point energy calculation was done using a larger basis set (B97D/def2QZVPP) to minimize the basis-set superposition error (BSSE). All energies were corrected for the zero-point vibrational energies. Additionally, Gibbs free energies (G) of TFA monomers and solvated monomers were computed respectively, as the sum of single-point energy (E_{EN}) of the equilibrium geometry, vibrational zero-point energy (E^0_{vib}), and thermal free-energy correction ($G_{\text{corr}}(T)$) at the gas-phase standard state (1 atm).

Crystal structures of TFA forms I and II were obtained from Cambridge Structure Database (refcode KAXXAI01 and KAXXAI) and then fully optimized to determine hydrogen

DOI: 10.1021/acs.jpcb.7b07763
J. Phys. Chem. B 2017, 121, 10118−10124

positions in the solid-phase structure by Crystal 14[17,18] at the level of pw1pw1/6-21g(d,p).[19]

Crystallization Experiments. Crystallization of TFA in DMF was carried out by crash cooling at various temperatures and supersaturations. The experiments were conducted in a 30 mL jacketed vessel with magnetic stirring at 200 rpm. Solutions at different concentrations were prepared by dissolving known amounts of TFA in DMF at elevated temperature. Upon complete dissolution, the solutions were withdrawn, filtered through a preheated 0.2 μm syringe filter, and transferred into the jacketed vessel and held at constant elevated temperature for 30 min. On transfer to a second temperature-controlled water circulator (Julabo FP50, Germany), the solution was rapidly cooled to the desired crystallization temperature within 2 min. Upon crystallization, the crystals were immediately filtered and analyzed by PXRD and/or FTIR.

RESULTS

Crystallization and Crystal Packing. In DMF, our experiments showed that TFA crystallizes into a solvate regardless of supersaturation or temperature (Supporting Information). The molecule shows the TL conformation (Table S2) and forms hydrogen bonds to DMF (Figure 2b). Crystallization from toluene or ethanol generally yields forms I, II, or both, depending on supersaturation levels.[10,20] The crystal structures bear three types of dimer motifs (Figure 3). One is

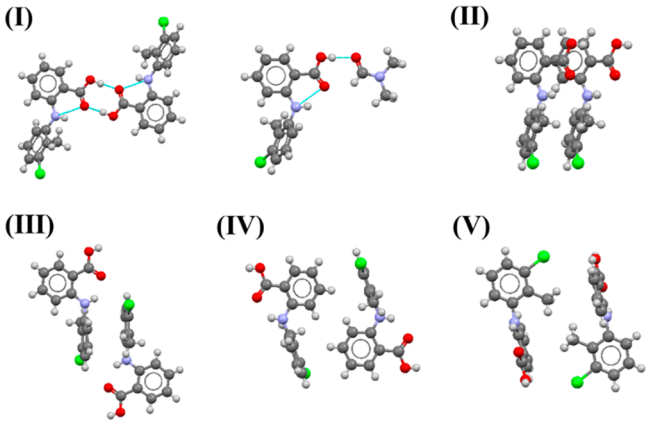

Figure 3. Geometries of optimized dimer motifs: (I) hydrogen-bonded homodimer (left) and heterodimer (right); (II) stacked dimer with two $\pi\cdots\pi$interactions; (III–V) CH$\cdots\pi$ or $\pi\cdots\pi$ stacked dimers.

the TFA–TFA carboxyl homodimer of PL or TL (Figure 3I, left); the second is TFA–DMF heterodimer of PL or TL (I, right); and the third is TFA-TFA stacked dimer through $\pi\cdots\pi$ and/or –CH$\cdots\pi$ interactions either by matching both anthranilic and chlorinated phenyl rings (II) or forming an inversion center (III–V).

TFA is a conformationally flexible molecule;[10,14,21] from the energy calculation of possible conformers and solvated monomers in toluene, DMF, and ethanol with an implicit solvation model (Table S3), it shows that (solvated) PL monomers are energetically more favorable than twisted ones. The interaction energy of solvated monomers is stronger than that of unsolvated ones. The interaction of TFA–DMF is significantly stronger, by about 10 kJ mol^{-1}, than that of TFA–ethanol. This is expected because DMF is a better hydrogen-bonding acceptor. Formation of hydrogen-bonded homodimers is unfavorable in DMF and ethanol, but forming stacked $\pi\cdots\pi$ dimers is desired (Figure S2). The energy per hydrogen bond of the solvated monomer in ethanol or DMF is stronger, by about 5 or 12 kJ mol^{-1}, than that of the homodimer. The interaction energy of the $\pi\cdots\pi$ stacked dimer between chlorinated phenyl rings (Figure 3III) is the strongest among all of the CH$\cdots\pi$ and $\pi\cdots\pi$ stacked dimers.

NMR and FTIR Spectroscopy. ^{1}H NMR chemical shifts are concentration-dependent in toluene-d_8 (Figure 4a). All aromatic protons except for H_{30} display downfield changes when the concentration increases, indicative of self-association. NH and H_7 show the largest changes, implying that the self-association is facilitated by hydrogen bonding formed between carboxyl groups. The C=O ^{13}C chemical shift indeed reveals downfield changes upon increase in TFA concentration (Figure S4a). IR spectra display two asymmetric C=O bands of TFA, 1663 and 1697 cm^{-1}, in toluene, and their intensity ratio is concentration-dependent (Figure 4d). The splitting of the C=O band results from two distinct solute species; the lower frequency band stems from the hydrogen bonding between TFA molecules and the other is of monomeric TFA. The concentration-dependent intensity ratio of the two bands corroborates the dimerization of TFA in toluene.

Chemical shift became dramatically different in DMF-d_7, and the trend suggests two concentration-dependent events (Figure 4b). The increase at low concentrations of the aromatic protons (H_9, H_{15}, H_{29}, H_{22}, and H_{28}) and decrease of the rest (H_7, H_{30}, and CH_3; NH not shown) were caused by ionization of TFA, which led to the downfield shift (deshielding) of C=O ^{13}C resonance, especially below 38 mM (the first event, Figure S4b). The deshielding of carbonyl ^{13}C upon ionization has been well documented in the literature and found significant in aqueous solution but dissipating rapidly in organic solvents.[22,23] The belief of ionization was further supported by significant line broadening of ^{1}H NMR when the concentration was further diluted (Figures S5). The C=O ^{13}C chemical shift was constant at concentrations above 38 mM (the second event), suggesting the absence of C=O in acting as a hydrogen-bond acceptor in solution. Nonetheless, concentration-dependent upfield changes of aromatic protons are observed, indicative of formation of aromatic stacking associates in solution. Solution FTIR spectra in DMF over a similar concentration range (78–470 mM) to the NMR experiments were collected (Figure 4e). Two C=O stretching bands were detected, a sharp peak at 1635 cm^{-1} and a broad one around 1669 cm^{-1}. The higher frequency band is of TFA C=O, and the other is of the solvent. Detailed IR band assignments can be found in Figure S6. Compared with the C=O stretching of pure solvent (1678 cm^{-1}),[24] the red shift of DMF carbonyl band in solution indicates the formation of TFA-DMF hydrogen bonding. As the concentration increases, the aromatic ring –C–H deformation reveals band shifts from 776 to 774 cm^{-1} and from 758 to 756 cm^{-1}, toward their values in the solid-state IR spectrum (Figure S7). These changes are due to aromatic interactions and TFA–TFA stacking in the solvent. In ethanol-d_6, the protons and carbonyl ^{13}C of TFA unveil similar concentration-dependent changes to those seen in DMF-d_7 (Figures 4c and S4c). The initial increase is seen for the same aromatic protons (H_9, H_{15}, H_{29}, H_{22}, and H_{28}) and the decrease for the remaining (H_7, H_{30}, and CH_3) at low concentrations. In the second event, a decrease is seen for all of the aromatic protons except for H_7. The only difference between the two solvents is for H_{30} and CH_3 in the second event. Solution IR spectra in ethanol exhibit two C=O bands (Figure 4f); the

DOI: 10.1021/acs.jpcb.7b07763
J. Phys. Chem. B 2017, 121, 10118–10124

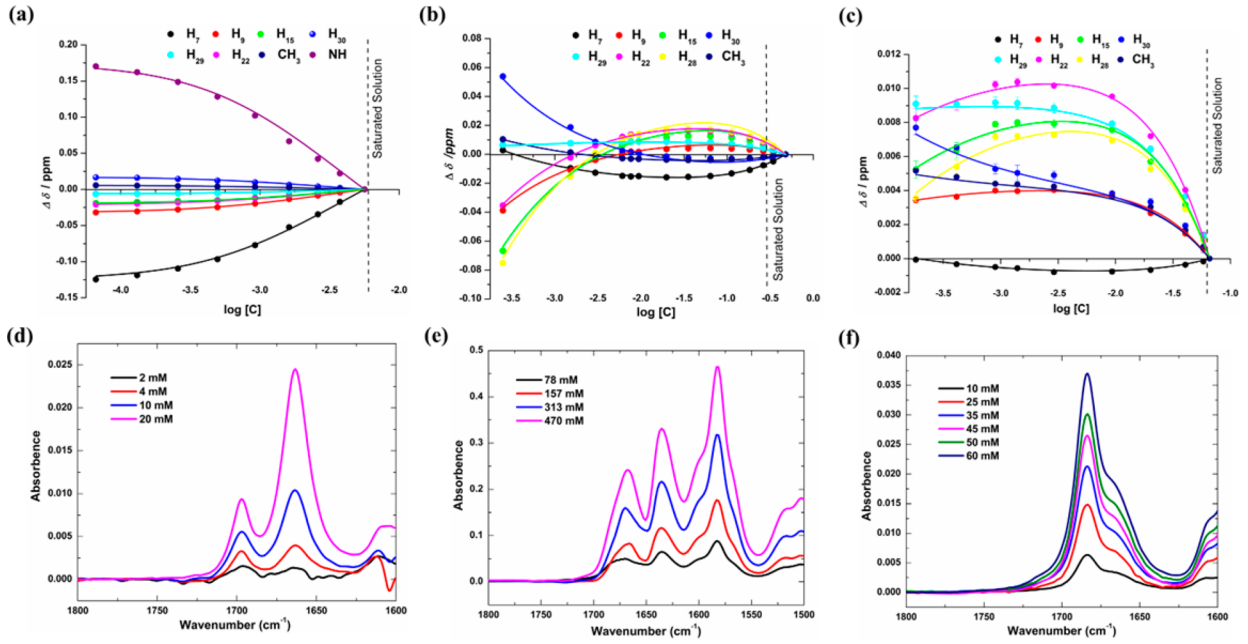

Figure 4. Top: ^{1}H NMR chemical shift changes of TFA as a function of concentration in toluene-d_8 (a), DMF-d_7 (b), and ethanol-d_6 (c) at 298 K. The lines in panel a are the best fit to a dimerization model, and in panels b and c are the best fit to a combined ionization and dimerization model. See Figure 1 for proton labeling. Bottom: FTIR spectra of TFA solutions in toluene (d), DMF (e), and ethanol (f) of a series of concentrations.

lower belongs to hydrogen-bonded C═O species, while the other can be of either non-hydrogen-bonded or hydrogen-bonded (through hydroxyl-hydroxyl interaction) carboxyl species. The simultaneous red shift upon deuteration of ethanol solvent (Figure S8) further confirms the two bands are of TFA−ethanol hydrogen-bonded pairs. In all, both NMR and IR data suggest the presence stacking associates that form hydrogen bonding with the solvents.

2D NOESY Spectra. The structural details of these solute−solute and solute−solvent assemblies were further explored by NOE measurement. 2D NOESY plots of TFA in toluene-d_8 display a comprehensive map of close contacts between intramolecular and intermolecular protons (Figure 5a,b). As expected, the NOE cross-peaks show opposite phases along the diagonal. Significant cross correlations between aromatic protons, including H_7−H_9, H_{30}−H_{29}, between H_{30} and methyl protons, and between H_{29} and NH, are identifiable in the plots. The stronger NOE signals indicate that H_{30} remains in close vicinity to methyl protons and much closer to H_{29}, implying the PL conformation where H_{30} is in close contact with H_{29} in the solution (2.26 Å from the optimized structure). It is also likely that TL also exists in solution (2.91 Å from the optimized structure) in which H_{30} stays close to methyl protons. Similarly, the 2D NOESY plot of TFA in DMF-d_7 displays the relatively strong cross-peaks between aromatic protons (H_7−H_9 and H_{30}−H_{29}) and between H_{30} and methyl protons. The results point out the presence of both PL and TL conformations (Figure 5c,d). The stronger H_{30}−H_{29} NOE hints that PL is dominant. More interestingly, spatial correlation between methyl protons and H_{22}/H_{28} can be identified in the plot. Both H_{22} and H_{28} are located at the opposite side of the same phenyl ring, and the rigid phenyl ring separates the methyl protons from H_{22} by about 6 Å of the same molecule. The NOE between the methyl protons and H_{22}/H_{28} can only result from intermolecular close contacts, likely due to the formation of stacking dimers (Figure 5, top). Note that the presence of TL or PL may be of the monomer, stacked dimer, or both species. Finally in ethanol-d_6, cross-peaks of CH_3−H_{30}, H_{30}−H_{29}, and CH_3−H_{22}/H_{28} are seen in 2D NOESY spectra (Figure 5e,f). Similar to DMF-d_7, the NOE data suggest that both TL and PL exist in ethanol and TFA stacked dimers between chlorinated phenyl rings are formed in the solution.

DISCUSSION

Solute Association and Conformation. The experimental data indicate distinct solute−solvent interactions and self-assemblies of TFA in the three solvents. In toluene-d_8, the solute self-assembles through hydrogen bonding, indicated by ^{1}H NMR measurements (Figure 4a), the downfield shift of C═O ^{13}C chemical shift (Figure S4a), and two well-separated concentration-dependent C═O IR bands (Figure 4d). The ^{1}H chemical shifts can be fit to a dimerization isotherm model (lines in Figure 4a), yielding a large self-association constant (149 ± 14 M^{-1}). Both PL and TL conformations are revealed in solution by NOE measurements (Figure 5a,b), with the overall conformation shifting from TL to PL evident by the decrease in the cross-peak volume ratio of CH_3−H_{30} and NH−H_{29} over H_7−H_9 (Figure S9a). The cross-peak volume ratios can be fit to a dimerization model, yielding the CH_3−H_{30} distance of 3.46 and 3.98 Å in the monomeric and dimeric states, respectively (Table S5). The molar fractions of PL and TL can be further estimated as 89% and 11% in the monomer state and 97% and 3% in the dimer state. The PL conformation clearly dominates regardless of the self-associate state of TFA.

TFA behaves differently in DMF. Strong solute−solvent interactions become apparent from the higher energy of TFA C═O stretching and red shift of the DMF C═O band (Figure 4e). The stronger solute−solvent hydrogen bonding dismisses any significant solute−solute hydrogen bonding. Aromatic stacking between TFA molecules is revealed by the solution ^{1}H NMR results (Figure 4b), the red shift of aromatic −C-H deformation IR bands (Figure S7), and most evidently, by the NOE between H_{22}/H_{28} and methyl protons (Figure 5b). The

DOI: 10.1021/acs.jpcb.7b07763
J. Phys. Chem. B 2017, 121, 10118−10124

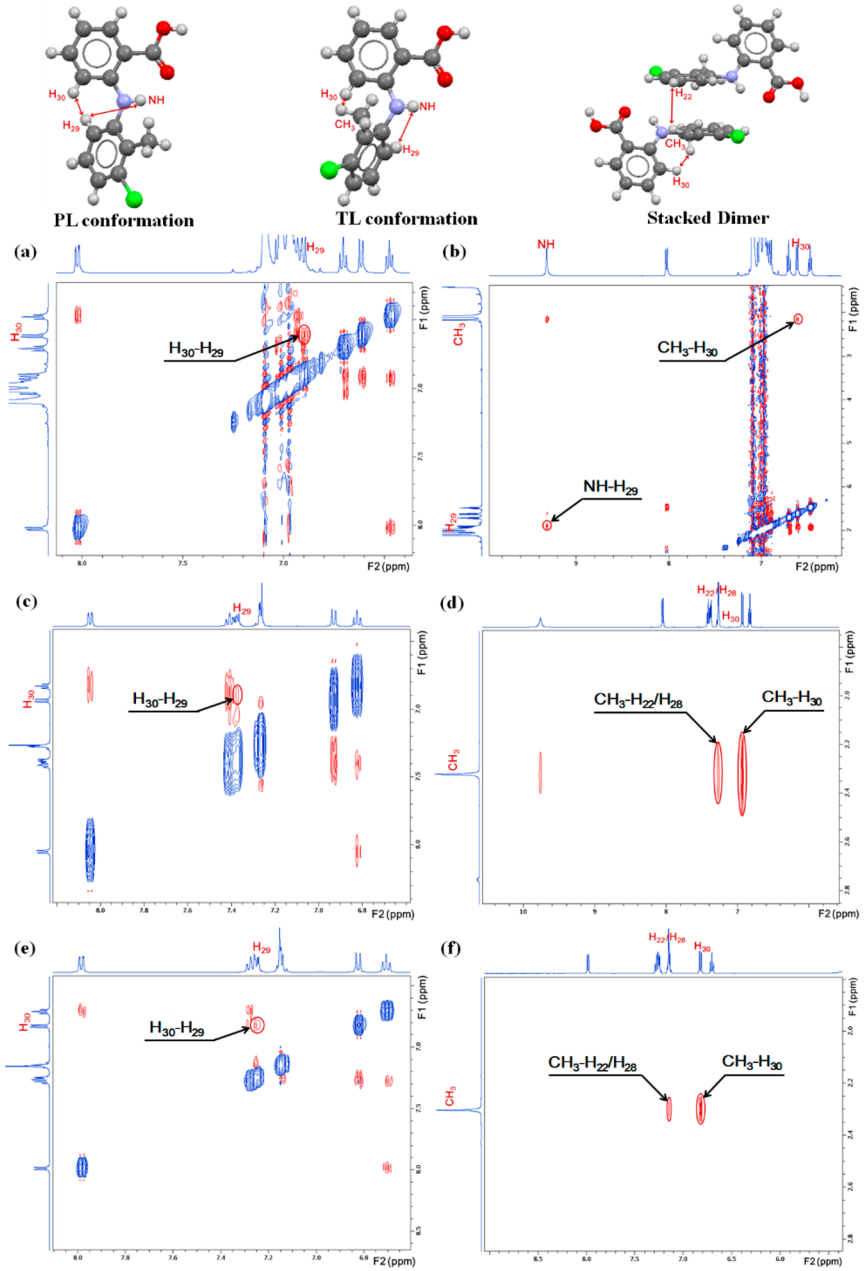

Figure 5. Top: optimized planar-like (PL) and twisted-like (TL) conformations as well as stacked dimer with selected interproton NOE labeled. (a and b): 2D NOESY plot of 4.5 mM TFA in toluene-d_8; (c and d): 511.6 mM TFA in in DMF-d_7; (e and f): 78.8 mM TFA in ethanol-d_6 at 298 K. Positive and negative signals are represented by blue and red contours, respectively.

proton chemical shifts can be fit into a combined ionization and dimerization isotherm model (lines in Figure 4b). In addition, the overall conformational population shifts to the TL conformation, as seen by the increase, albeit small, in the cross-peak volume ratio of CH_3−H_{30} over H_7−H_9 as the concentration increases (Figure S9b). The change in cross-peak volume ratios can be fit to a dimerization model, yielding the stacking dimerization constant of 0.13 ± 0.01 M^{-1} and molar ratio between PL and TL of 18.3. This suggests that in DMF, TFA adopts conformations that are flat or planar. In ethanol, the solution chemistry is similar to that in DMF. The two concentration-dependent trends of ^{1}H chemical shift (Figure 4c) resulted respectively from ionization and self-association and can be fitted to an isotherm model (lines in Figure 4c). The solute indeed engages in hydrogen bonding with ethanol, as indicated by the two C═O bands in solution IR; the lack of concentration-dependence of the two bands further suggests no significant hydrogen bonding formed between TFAs. The TFA−ethanol hydrogen bonding is calculated to be much stronger than that of TFA−TFA homodimers. Intermolecular stacking was detected by NOE between TFA aromatic rings, indicated by the increase in cross-peak volume ratio of CH_3−H_{22}/H_{28} or CH_3−H_{30} over H_7−H_9 (Figure S9c). Fitting the cross-peak volume ratios to a dimerization model results in the stacking dimerization constant of 0.59 ± 0.05 M^{-1} and the PL/TL ratio 15.7. Again, the planar conformation is dominant in ethanol. Overall, depending on the solvent, TFA can form either strong self-associates via hydrogen bonding as in toluene or weaker $\pi\cdots\pi$ stacking while forming hydrogen bond with DMF or ethanol. The self-association constant in toluene, 149

DOI: 10.1021/acs.jpcb.7b07763
J. Phys. Chem. B 2017, 121, 10118−10124

M^{-1}, dwarfs those in the other two solvents (0.13 and 0.59 M^{-1}). The planar conformation becomes much more preferred in DMF and ethanol than in toluene, possibly to enforce the solute−solvent hydrogen bonding.

Connection between Solution Chemistry and Crystallization Outcome. The solution chemistry could shed light on the nucleation mechanism. The hydrogen-bonded TFA homodimers formed in toluene seem to be preserved in the resultant crystal structures; both PL and TL conformers coexist in the solution, and the two crystal forms differ only in the molecular conformation, which resembles either PL or TL. In DMF, TFA hydrogen bonds with the solvent in solution and the crystal contains the TFA−DMF pair. Additionally, the $\pi\cdots\pi$ stacking between TFA molecules is observed in the solution as well as in the crystal structure. It is thus tempting to speculate that nucleation may proceed by high-order clusters and subsequent attachment by the solvated solute species in toluene or DMF. Nonetheless, there seems to be no structural linkage when TFA crystallizes in ethanol, in which the solute forms hydrogen bonding with ethanol and, concurrently, self-associates via weaker aromatic interactions in solution. The resultant crystal structures, however, contain no crystallographic ethanol but the same TFA−TFA hydrogen-bonded homodimers as in the crystals produced from toluene. It is thus argued that the prenucleating, solvated TFA aggregates in ethanol undergo supramolecular reconstruction to detach solvent molecules and build up dense TFA-only nuclei that enable hydrogen bonding formed between the solute molecules. It is possible that initial clusters are formed by ethanol-bonded TFA molecules and then transform via desolvation into TFA−TFA clusters that eventually result in stable nuclei for growth. Apparently, desolvation or removal of ethanol molecules from the nucleating, supramolecular clusters could be a necessary step to reconcile the ostensible discrepancy between the solution chemistry and crystallization outcome in ethanol.

While our speculation of nucleation mechanism warrants further investigation, the differences and similarities in the solution chemistry of TFA in the three distinct solvents highlight the significance of the interplay between solute−solute and solute−solvent interactions in driving the self-assembly process. Whether or not a solution species is preserved through crystallization results from such interplay and likely influences the structural evolvement in nuclei.

CONCLUSIONS

Nucleation of organic molecules is and will remain elusive to study. Understanding the solution chemistry will provide a critical glimpse into the elusive nature of the event. What is revealed by our study is that the solute self-assembles as the concentration increases, even if such a self-assembly is fostered by weaker, secondary intermolecular forces while the solvent picks up the primary one such as hydrogen bonding. Whether or not there is a direct structural similarity or link between the solution chemistry and crystal structure, the self-assembly likely determines how a nucleus forms and evolves leading to crystal formation.

ASSOCIATED CONTENT

Supporting Information

The Supporting Information is available free of charge on the ACS Publications website at DOI: 10.1021/acs.jpcb.7b07763.

Solubility, crystallization trajectories and results, and crystallographic data (Tables S1 and S2 and Figure S1); energy calculations (Table S3 and Figure S2); HMBC, concentration-dependent TFA C═O ^{13}C chemical shift data, dilution ^{1}NMR, and IR spectra (Figures S3−S8); fitting models and results of TFA chemical shifts as a function of concentration (Table S4); NOE quantification model and data (Figure S9 and Table S5). (PDF)

AUTHOR INFORMATION

Corresponding Authors

*E-mail: junbo_gong@tju.edu.cn.
*E-mail: tonglei@purdue.edu.

ORCID

Junbo Gong: 0000-0002-3376-3296
Tonglei Li: 0000-0003-2491-0263

Notes

The authors declare no competing financial interest.

ACKNOWLEDGMENTS

W.T. acknowledges funding support from the China Scholarship Council (CSC) and the National Natural Science Foundation of China (NSFC; Nos. 21676179 and 91634117). The work was also supported by Chao Endowment at Purdue University.

REFERENCES

(1) Khamar, D.; Zeglinski, J.; Mealey, D.; Rasmuson, Å. C. Investigating the Role of Solvent−Solute Interaction in Crystal Nucleation of Salicylic Acid from Organic Solvents. *J. Am. Chem. Soc.* **2014**, *136*, 11664−11673.

(2) Gibson, J. M.; Popham, J. M.; Raghunathan, V.; Stayton, P. S.; Drobny, G. P. A Solid-State NMR Study of the Dynamics and Interactions of Phenylalanine Rings in a Statherin Fragment Bound to Hydroxyapatite Crystals. *J. Am. Chem. Soc.* **2006**, *128*, 5364−5370.

(3) Davey, R. J.; Schroeder, S. L.; ter Horst, J. H. Nucleation of Organic Crystals—A Molecular Perspective. *Angew. Chem., Int. Ed.* **2013**, *52*, 2166−2179.

(4) Davey, R.; Dent, G.; Mughal, R.; Parveen, S. Concerning the Relationship between Structural and Growth Synthons in Crystal Nucleation: Solution and Crystal Chemistry of Carboxylic Acids as Revealed through IR Spectroscopy. *Cryst. Growth Des.* **2006**, *6*, 1788−1796.

(5) Lohani, S.; Nesmelova, I. V.; Suryanarayanan, R.; Grant, D. J. W. Spectroscopic Characterization of Molecular Aggregates in Solutions: Impact on Crystallization of Indomethacin Polymorphs from Acetonitrile and Ethanol. *Cryst. Growth Des.* **2011**, *11*, 2368−2378.

(6) Gidalevitz, D.; Feidenhans'l, R.; Matlis, S.; Smilgies, D.-M.; Christensen, M. J.; Leiserowitz, L. Monitoring in Situ Growth and Dissolution of Molecular Crystals: Towards Determination of the Growth Units. *Angew. Chem., Int. Ed. Engl.* **1997**, *36*, 955−959.

(7) Chattopadhyay, S.; Erdemir, D.; Evans, J. M. B.; Ilavsky, J.; Amenitsch, H.; Segre, C. U.; Myerson, A. S. SAXS Study of the Nucleation of Glycine Crystals from a Supersaturated Solution. *Cryst. Growth Des.* **2005**, *5*, 523−527.

(8) Huang, J.; Stringfellow, T. C.; Yu, L. Glycine Exists Mainly as Monomers, Not Dimers, in Supersaturated Aqueous Solutions: Implications for Understanding Its Crystallization and Polymorphism. *J. Am. Chem. Soc.* **2008**, *130*, 13973−13980.

(9) Kellermeier, M.; Rosenberg, R.; Moise, A.; Anders, U.; Przybylski, M.; Colfen, H. Amino Acids Form Prenucleation Clusters: ESI-MS as a Fast Detection Method in Comparison to Analytical Ultracentrifugation. *Faraday Discuss.* **2012**, *159*, 23−45.

(10) Du, W.; Cruz-Cabeza, A.; Woutersen, S.; Davey, R.; Yin, Q. Can the Study of Self-Assembly in Solution Lead to a Good Model for the

DOI: 10.1021/acs.jpcb.7b07763
J. Phys. Chem. B 2017, 121, 10118−10124

Nucleation Pathway? The Case of Tolfenamic Acid. *Chem. Sci.* **2015**, *6*, 3515−3524.
(11) Andersen, K. V.; Larsen, S.; Alhede, B.; Gelting, N.; Buchardt, O. Characterization of Two Polymorphic Forms of Tolfenamic Acid, N-(2-Methyl-3-Chlorophenyl)Anthranilic Acid: Their Crystal Structures and Relative Stabilities. *J. Chem. Soc., Perkin Trans. 2* **1989**, 1443−1447.
(12) López-Mejías, V.; Kampf, J. W.; Matzger, A. J. Polymer-Induced Heteronucleation of Tolfenamic Acid: Structural Investigation of a Pentamorph. *J. Am. Chem. Soc.* **2009**, *131*, 4554−4555.
(13) Vögeli, B. The Nuclear Overhauser Effect from a Quantitative Perspective. *Prog. Nucl. Magn. Reson. Spectrosc.* **2014**, *78*, 1−46.
(14) Mattei, A.; Mei, X.; Miller, A. F.; Li, T. Two Major Pre-Nucleation Species That Are Conformationally Distinct and in Equilibrium of Self-Association. *Cryst. Growth Des.* **2013**, *13*, 3303−3307.
(15) Frisch, M. J.; et al. *Gaussian 09*, Gaussian, Inc.: Wallingford, CT, 2009.
(16) Pratt, L. M.; Truhlar, D. G.; Cramer, C. J.; Kass, S. R.; Thompson, J. D.; Xidos, J. D. Aggregation of Alkyllithiums in Tetrahydrofuran. *J. Org. Chem.* **2007**, *72*, 2962−2966.
(17) Dovesi, R.; Orlando, R.; Erba, A.; Zicovich-Wilson, C. M.; Civalleri, B.; Casassa, S.; Maschio, L.; Ferrabone, M.; De La Pierre, M.; D'Arco, P.; Noël, Y.; Causà, M.; Rérat, M.; Kirtman, B. Crystal14: A Program for the ab Initio Investigation of Crystalline Solids. *Int. J. Quantum Chem.* **2014**, *114*, 1287−1317.
(18) Dovesi, R.; Saunders, V.; Roetti, C.; Orlando, R.; Zicovich-Wilson, C.; Pascale, F.; Civalleri, B.; Doll, K.; Harrison, N.; Bush, I. *Crystal14 User's Manual*; University of Torino: Torino, Italy, 2014.
(19) Perdew, J. P.; Chevary, J. A.; Vosko, S. H.; Jackson, K. A.; Pederson, M. R.; Singh, D. J.; Fiolhais, C. Atoms, Molecules, Solids, and Surfaces: Applications of the Generalized Gradient Approximation for Exchange and Correlation. *Phys. Rev. B: Condens. Matter Mater. Phys.* **1992**, *46*, 6671−6687.
(20) Mattei, A.; Li, T. Polymorph Formation and Nucleation Mechanism of Tolfenamic Acid in Solution: An Investigation of Pre-Nucleation Solute Association. *Pharm. Res.* **2012**, *29*, 460−470.
(21) Mattei, A.; Li, T. Interplay between Molecular Conformation and Intermolecular Interactions in Conformational Polymorphism: A Molecular Perspective from Electronic Calculations of Tolfenamic Acid. *Int. J. Pharm.* **2011**, *418*, 179−186.
(22) Hagen, R.; Roberts, J. D. Nuclear Magnetic Resonance Spectroscopy. ^{13}C Spectra of Aliphatic Carboxylic Acids and Carboxylate Anions. *J. Am. Chem. Soc.* **1969**, *91*, 4504−4506.
(23) Holmes, D. L.; Lightner, D. A. Synthesis and Acidity Constants of $^{13}CO_2H$-Labelled Mono and Dipyrrole Carboxylic Acids. pK_a from ^{13}C-NMR. *Tetrahedron* **1996**, *52*, 5319−5338.
(24) Sharma, A.; Kaur, S.; Mahajan, C. G.; Tripathi, S. K.; Saini, G. S. S. Fourier Transform Infrared Spectral Study of N,N′-Dimethylformamide-Water-Rhodamine 6G Mixture. *Mol. Phys.* **2007**, *105*, 117−123.

DOI: 10.1021/acs.jpcb.7b07763
J. Phys. Chem. B 2017, 121, 10118−10124